Multiplex coherent anti-Stokes Raman spectroscopy study of infrared-multiphoton-excited OCS

Kuei-Hsien Chen, Cheng-Zai Lü, Luis A. Avilés,[a] Eric Mazur, and Nicolaas Bloembergen
Division of Applied Sciences, Harvard University, Cambridge, Massachusetts 02138

Mary J. Shultz
Department of Chemistry, Tufts University, Medford, Maryland 02155, and George R. Harrison Spectroscopy Laboratory, MIT, Cambridge, Massachusetts 02139

(Received 27 January 1989; accepted 19 April 1989)

The vibrational energy distribution following ν_2 overtone excitation of OCS by a pulsed CO_2 laser is studied by monitoring the coherent anti-stokes Raman spectrum of the ν_1 mode. Because of the slow energy transfer from the pumped mode to other modes, and because the anharmonicity of the ν_2 mode is small, OCS is an ideal system for studying the interaction of an intense infrared laser field with a single, nearly harmonic, oscillator. From the spectra the cross anharmonicities of the ν_1 mode are determined to be $x_{12} = -6.0\ \mathrm{cm}^{-1}$ and $x_{13} = -2.7\ \mathrm{cm}^{-1}$, respectively. The time dependence of the spectra provides information on V–V energy transfer rates. In particular, the measurements put a lower limit of $k_{\nu_2 \to \nu_2} = 1\ \mu\mathrm{s}^{-1}\ \mathrm{Torr}^{-1}$ on the vibrational relaxation rate within ν_2 mode. At high excitation, the temperature of the ν_2 mode rises up to 2000 K, and hot bands are observed up to the $n = 4$ level. This fourth overtone peak is split because of either a Fermi resonance or vibrational angular momentum splitting.

I. INTRODUCTION

The discovery of infrared multiphoton excitation[1] led to a large experimental[2,3] and theoretical[4] research effort aimed at understanding this phenomenon. Although the gross features of infrared multiphoton are now well understood, more detailed, quantitative spectroscopic information is needed to understand the mechanism of the excitation and the related intramolecular vibrational relaxation processes. In the past few years time-resolved spontaneous Raman spectroscopy experiments have provided information on the vibrational energy distributions of infrared-multiphoton-excited molecules.[3,5,6]

Nonlinear optical techniques[7] make it possible to improve the probing, and to provide more quantitative results. For instance, coherent anti-Stokes Raman spectroscopy (CARS), which has a wide spectral range and high temporal and spectral resolution, is a particularly good technique for studying infrared multiphoton excitation.[8–10] Because of the high signal level, CARS is much more sensitive than spontaneous Raman spectroscopy. In addition, using a folded BOXCARS beam geometry[11] one obtains a high spatial resolution. This not only eliminates the signal from molecules outside of the region pumped by the infrared laser, but also the nonresonant signal from the cell windows. Finally, with *multiplex* CARS probing[12] one can obtain the entire spectrum in a single laser shot and prevent problems associated with laser power fluctuations. All these fundamental advantages over spontaneous Raman make multiplex BOXCARS an excellent technique for studying infrared multiphoton excitation.

This paper reports on multiplex BOXCARS measurements of the state-specific population distribution of OCS following infrared irradiation by a CO_2 laser. The OCS molecule has three widely separated fundamental modes ($\nu_1 = 859\ \mathrm{cm}^{-1}$, $\nu_2 = 527\ \mathrm{cm}^{-1}$, $\nu_3 = 2079\ \mathrm{cm}^{-1}$). The overtone of the ν_2 mode can be excited with CO_2 laser frequencies between the $P(10)$ and $P(26)$ lines of the 9.6 μm branch. Because of the wide separation of the vibrational modes of OCS, and also because of a low density of states, the intramolecular vibrational energy transfer is very inefficient.[13] In contrast, pumping and population redistribution within the ν_2 bending mode, excited by the CO_2 laser, is very efficient owing to the small anharmonicity. Thus, OCS is an ideal molecule for studying the interaction of a single anharmonic oscillator with an intense infrared laser field.

Since there are many excellent reviews of the CARS technique,[14–16] only the essential details will be given here. In the next section, the theory of CARS scattering intensity, the multiplex detection, and the folded BOXCARS geometry, will be reviewed. The subsequent sections present the experimental arrangement and experimental data, and a full discussion of the results obtained.

II. THEORY

In the coherent anti-Stokes Raman process, three photons, two at frequencies ω_1 and one at ω_2, coherently interact with the molecules through the third-order nonlinear susceptibility $\chi^{(3)}$. The coherent interaction generates a polarization at $\omega_C = 2\omega_1 - \omega_2$, which in turn gives rise to a coherent signal[17]

$$I(\omega_C) \propto I^2(\omega_1) I(\omega_2) |\chi^{(3)}(-\omega_C, \omega_1, \omega_1, -\omega_2)|^2 (\Delta z^2), \quad (1)$$

where the $I(\omega)$ are the intensities of the laser beams and Δz is the interaction length. The third order susceptibility $\chi^{(3)}$ can be expressed as

[a] Bell Communications Research student.

 0021-9606/89/151462-07$02.10

$$\chi^{(3)} \propto \Delta N\left(\frac{d\sigma}{d\Omega}\right), \tag{2}$$

where ΔN is the population difference between the two Raman transition states of the molecule, and $(d\sigma/d\Omega)$ the Raman cross section. By conservation of energy and momentum, we have

$$\omega_C = 2\omega_1 - \omega_2, \tag{3}$$

and

$$\mathbf{k}_C = 2\mathbf{k}_1 - \mathbf{k}_2, \tag{4}$$

respectively, where the $\mathbf{k}$ are the corresponding wave vectors. Equations (3) and (4) show the main advantages of coherent anti-Stokes spectroscopy. First, as can be seen from Fig. 1(a), the spectral resolution is determined by the bandwidth of the lasers at ω_1 and ω_2. Second, momentum conservation confines the coherent anti-Stokes photon to a small solid angle, thus, greatly facilitating signal collection relative to spontaneous Raman scattering.

There are several phase matching geometries satisfying Eq. (4): collinear CARS, BOXCARS, and folded BOXCARS. Of these, the folded BOXCARS arrangement shown in Fig. 2, with the two ω_1 beams in one plane, and ω_2 and ω_C in another plane perpendicular to it, provides optimal separation of the CARS signal from the input laser beams, greatly improving the signal-to-noise ratio. Also, spatial resolution is very high since the signal is generated only in the overlap region between the ω_1 and ω_2 beams. As Fig. 2 shows, this geometry allows one to probe within the width of the exciting infrared laser beam, thus excluding signal from "cold" molecules outside the infrared laser beam, and at the same time eliminating any nonresonant signal from the glass windows.

The alignment of folded BOXCARS can be done routinely in a few minutes as follows. First, the phase matching angle for the laser beams is calculated. Second, from these angles, the location of each beam in front of the focusing lens is marked using a plate with four pin holes. Then, the laser beams are aligned through the pin holes in such a way that they are perfectly parallel to each other. Next, a He–Ne laser is aligned along the calculated direction of the CARS beam. After the focusing lens is put in the path of the laser beams, overlap of the beam waists is optimized by looking at the elastic scattering from the ambient air in the overlap region. When the scattering cell is put into place in the scattering region, the CARS signal follows the He–Ne beam path. Using this procedure, for SF_6 at a pressure of 3 atm, the CARS signal can easily be detected by eye. This allows easy alignment of the detection optics and the spectrometer behind the scattering cell.

For a fixed ω_1, there are two methods for scanning the Raman spectrum. If ω_2 is a narrow band laser, the spectrum can be obtained by scanning the frequency ω_2 of the laser. The disadvantage of scanning is that since CARS is a nonlinear technique, jitter, both spatial and temporal, in the ω_1 and ω_2 lasers results in noise in the spectrum when it is collected a point at a time. Alternatively, one can use a broad band dye laser at ω_2, as illustrated in Fig. 1(b), in which case the entire CARS spectrum is generated simultaneously. In the latter case, called *multiplex* CARS, the spectrum is obtained by dispersing the CARS output beam through a monochromator and collecting the signal on a detector array. In contrast to scanning CARS, the entire spectrum can be obtained in a single laser shot, thus eliminating shot-to-shot intensity variations. Also, because of the much shorter data-acquisition time, the signal-to-noise can be greatly enhanced. On the other hand, one must sacrifice spectral resolution, which now is not determined by a convolution of the laser wavelengths, but by a convolution of the resolution of the dispersion monochromator, multiplex detector, and the line width of ω_1. For the purpose of this work, however, sufficient spectral resolution could be obtained with a high resolution spectrograph, and, therefore, the multiplex scheme was employed throughout the experiments.

III. SETUP

A schematic view of the setup is shown in Fig. 3. The infrared radiation is generated by a grating-tuned CO_2 laser with 250 ns pulse duration and a maximum energy of 200 mJ. For the $2\nu_2$ overtone excitation of OCS the laser was tuned to the $P(24)$ line of the 9.6 μm branch. The infrared beam is focused into the interaction cell by a cylindrical lens with a 15 cm focal length. The CARS laser beams are derived from the output of a Quantel YG471C Nd:YAG laser with 10 ns pulse duration and 200 mJ average second-harmonic output at 532 nm. About 50 mJ is used for the two ω_1 beams (25 mJ each), while the remainder serves to pump a broad band dye laser-amplifier system at ω_2. The prism tuned broad band laser, operating on Fluorescein 548 dye around 550 nm, produces 20 mJ pulses of 6 ns pulse duration, and 60 cm^{-1} linewidth. These pulses are amplified to 20 mJ in two

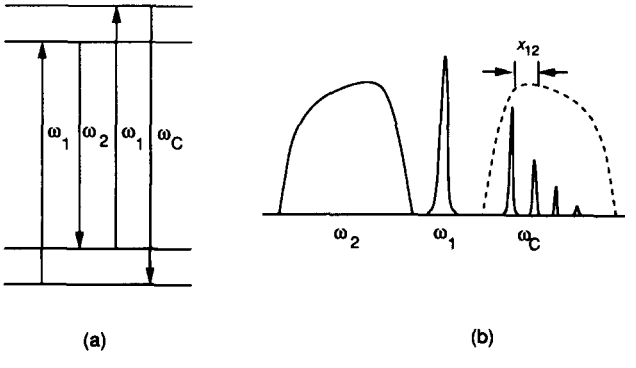

FIG. 1. (a) CARS energy level diagram, and (b) multiplex scheme.

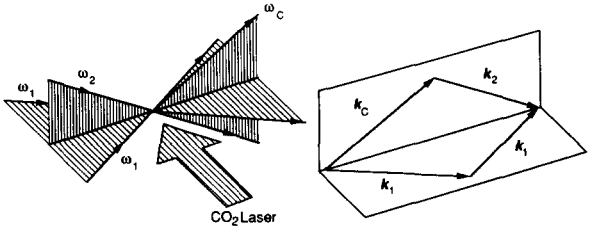

FIG. 2. BOXCARS beam configuration, and phase matching diagram.

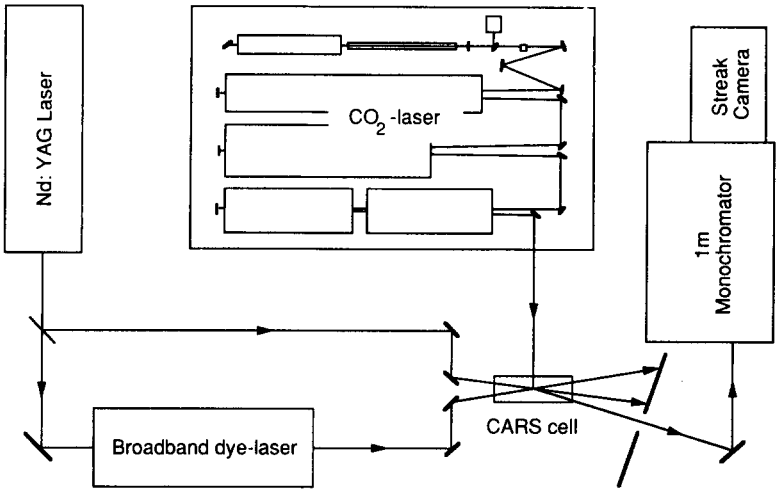

FIG. 3. Experimental setup.

stages. All the ω_1 and ω_2 beams are vertically polarized, and are aligned parallel to one another before being focused into the scattering cell with a 25 cm focal length lens. The infrared laser beam and the CARS laser beams cross at right angles inside the scattering cell. The beam waist and the interaction length of the CARS beams are 80 and 200 μm, respectively. The dimensions of the infrared pump beam in the interaction region are 110 μm and 18 mm, respectively.

The CARS beam generated in the interaction cell passes through an aperture which spatially rejects the ω_1 and ω_2 beams. A cutoff filter, which rejects light of wavelength longer than 520 nm, is used to further reduce the elastically scattered light from the windows and other background radiation. The signal is then dispersed using a Jarrel Ash 78-420 1 m f/6.2 monochromator with a 0.05 Å resolution in second order. Instead of using the output slit of the monochromator, the dispersed CARS signal is recorded on the (horizontal) entrance slit of a Hamamatsu C1587 streak camera system with a 512 by 512 detector array. The resulting spectral resolution of the entire system is 0.12 Å. The dispersion of the monochromator was calibrated with the 6 Å separation of the two Na D lines. For each spectrum an average over 50 shots is taken to obtain a good signal-to-noise ratio.

Because of the difficulty in accurate synchronization of the CO_2 and Nd:YAG lasers and the streak camera, the measurements presented here do not make use of the temporal resolution of the streak camera. Instead, time resolution was obtained by varying the delay between the pump and the probe pulses. The synchronization of the lasers is achieved electronically by controlling the timing between the Q switch of the Nd:YAG laser and the voltage drop of the high voltage discharge plates of the CO_2 laser. The time delay can be varied from 0 to 6 μs with a 20 ns jitter. In the near future we plan to improve this by making use of shorter (subnanosecond) infrared pulses and obtaining the timing information from the streak camera. In that case, both spectral and time dependence of the CARS signal can be obtained in a single shot.

A number of consistency checks was performed. First, it was verified that the signal only occurs in the presence of all three input laser beams. Second, by varying the pressure of the gas sample, it showed the CARS signal depends quadratically on the sample pressure as expected from the ΔN^2 dependence in Eqs. (1) and (2). However, when the intensity of the ω_1 or ω_2 beams was varied by putting neutral density filters in the laser beam paths, we could not obtain the expected relation between the CARS signal and intensities of the ω_1 and ω_2 beams as described in Eq. (1). This difficulty, which is common in all nonlinear optical technique, can be attributed to the fact that the beam overlap in the interaction region changes when filters are inserted in the laser beam paths.

IV. RESULTS AND ANALYSIS

The experimental results are shown in Figs. 4 through 7. The CARS spectrum of the ν_1 mode of OCS at room temperature is shown in Fig. 4. The right-most peak is the ground state peak for the ν_2 mode, and corresponds to the vibrational transition between the $(v_1,v_2,v_3) = (0,0,0)$ and $(1,0,0)$ states. The second peak from the right reflects the bending hot band $(0,1,0) \rightarrow (1,1,0)$ and the barely visible, left-most peak is due to the ground state of the ^{34}S isotope,

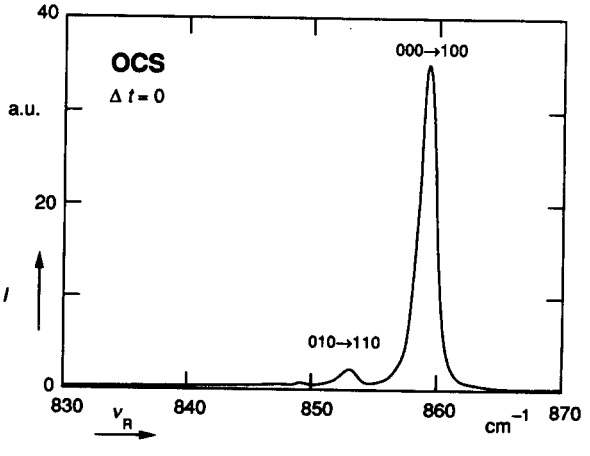

FIG. 4. CARS spectrum for OCS at $p = 100$ Torr and $T = 300$ K.

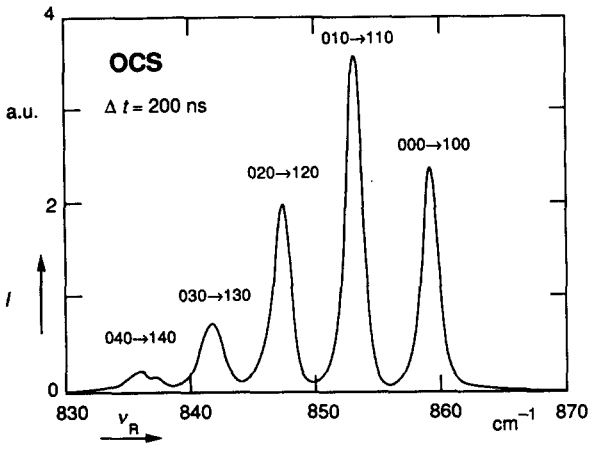

FIG. 5. CARS spectrum for OCS at $p = 100$ Torr, 200 ns after excitation. CO_2 laser fluence: 9.2 J/cm^2.

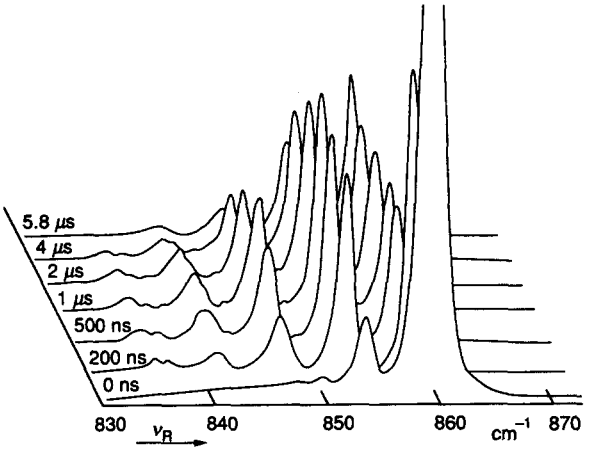

FIG. 7. CARS spectrum for OCS at $p = 50$ Torr, for various delay times after excitation. CO_2 laser fluence: 9.2 J/cm^2.

which has a 4% natural abundance. This ^{34}S ground state peak is just at the limit of the sensitivity of our apparatus.

After infrared excitation dramatic changes in the spectrum occur. Figure 5 shows a typical spectrum 200 ns after infrared excitation. A large decrease in the fundamental peak is observed (note the difference in vertical scale), and additional hot bands corresponding to excitation in the ν_2 ladder up to $\nu_2 = 4$ appear in the spectrum. This fourth overtone peak always appears to be split.

For longer delays the spectrum continues to change. Figure 6 shows the spectrum 4 μs after the infrared pump. In addition to the structure observed for short delay times, small peaks appear between the ν_2 hot bands. Each peak is also more asymmetric than the corresponding ones in Fig. 5.

The overall time evolution of the CARS spectrum at 50 Torr is shown in Fig. 7. Note that the strong ground state signal depletion for time $t < 1$ μs, and the slow recovery at longer time delays. In contrast, the other peaks in the ν_2 hot band grow and then decrease again. At the same time, the intensity of the additional small peaks in between the ν_2 hot band peaks increases with time.

The intensity distribution of the hot band peaks reflects the square of the population distribution in the ν_2 mode. Since CARS is a nonlinear technique, however, care must be exercised when determining the population distribution from the intensity distribution.[18] If the rotational lines are closely spaced, which is true for the Q branch spectra of molecules with a small rotational constant, the population distribution $N(E)$ can be obtained by taking the square root of the area within the full width half-maximum (FWHM) of each peak. For the room temperature spectrum shown in Fig. 4, the distribution thus obtained is in good agreement with a room temperature Boltzmann distribution. A comparison of the population distributions for infrared multiphoton excited OCS with Boltzmann distributions is shown in Fig. 8. The vertical axis plots the population N, obtained from the square root of the FWHM peak area as explained above, divided by the degeneracy $g = v_2 + 1$ of the corresponding level v_2. During the excitation, for a delay of 200

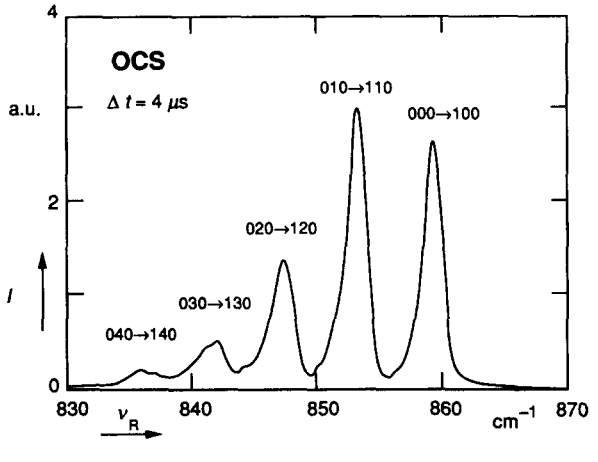

FIG. 6. CARS spectrum for OCS at $p = 100$ Torr, 4 μs after excitation. CO_2 laser fluence: 9.2 J/cm^2.

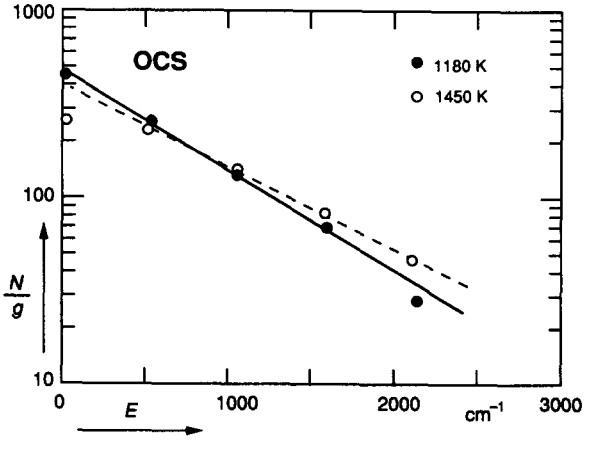

FIG. 8. Population distributions of the ν_2 mode of OCS at $p = 100$ Torr, 200 ns (●) and 500 ns (○) after CO_2 laser excitation (9.2 J/cm^2). The closed circles are from the spectrum in Fig. 5. The lines show Boltzmann fits for $T = 1200$ (plain) and $T = 1500$ (dashed).

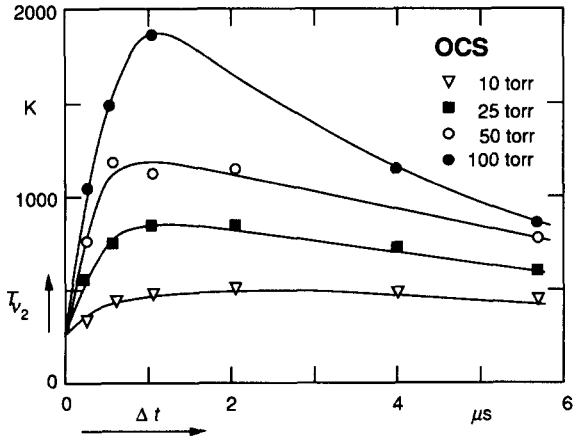

FIG. 9. Temperature of ν_2 mode vs delay time after a 9.2 J/cm^2 CO_2 laser excitation for different OCS pressures (∇: 10 Torr, ■: 25 Torr, ○: 50 Torr, ●: 100 Torr).

ns, the distribution is still in excellent agreement with a Boltzmann distribution at a temperature of 1200 K. At higher excitation, however, deviations from a Boltzmann distribution are observed. While the population of all but the ground state are still well described by a Boltzmann distribution at $T = 1500$ K, the $v_2 = 0$ state has a lower population than expected. Figure 9 shows the temperature evolution of the ν_2 mode for sample pressures ranging from 10 to 100 Torr.

The dependence of the excitation on the CO_2 laser wavelength was also investigated by tuning the laser from the $P(10)$ to $P(26)$ line on the 9.6 μm branch. The experiment was performed at a pressure of 70 Torr, a delay of 1 μs, and an infrared fluence of 7.6 J/cm^2. For each run the population distribution and temperature of the ν_2 mode was determined as described above. Where deviations from a Boltzmann distributions occurred, the best fit value was taken. The result is shown in Table I, together with the CO_2 laser excitation

TABLE I. Temperature of the ν_2 mode after excitation at different CO_2 lines. The energy mismatch between the laser wavelength and the closest rovibrational transition from Ref. 19. The population of the initial rotational state N_J is also given.

CO_2 laser line	Energy (cm^{-1})	OCS transition (0,0,0)→(0,2^0,0) (cm^{-1})		N_J	Mismatch (cm^{-1})	T_{v_2} (K)
$P(26)$	1041.28	P_{14}	1041.48	0.85	0.20	750
$P(24)$	1043.16	P_{10}	1043.04	0.68	0.12	900
$P(22)$	1045.02	P_5	1045.03	0.38	0.01	1050
$P(20)$	1046.85	P_1	1046.64	0.11	0.21	500
$P(18)$	1048.66	R_3	1048.68	0.25	0.02	800
$P(16)$	1050.44	R_7	1050.33	0.51	0.11	500
$P(14)$	1052.20	R_{11}	1052.01	0.73	0.19	550
$P(12)$	1053.92	R_{16}	1054.13	0.92	0.21	450
$P(10)$	1055.63	R_{20}	1055.85	0.99	0.22	450

wavelength, the closest rovibrational overtone transition,[19] the energy mismatch between them, as well as the room temperature population of the initial rotational state.

The data in the table clearly show that there is a correlation between the energy mismatch and the excitation temperature T_{v_2}. When the mismatch is small, the excitation is large. In addition, the population of the initial state also plays a role: the larger the population, the larger the fraction of excited molecules, and consequently the higher the excitation temperature. In addition to the mismatch listed in the table, the mismatch of higher lying transitions, such as the (0,1,0)→(0,3,0), and (0,2,0)→(0,4,0) transitions, also play a role.

V. DISCUSSION

The OCS spectra presented in the previous section provides information on the cross anharmonicities and the vibrational relaxation. The spectra are determined by the vibrational energy

$$E(v_1,v_2^l,v_3) = (v_1 + 1/2)h\nu_1 + (v_2 + 1)h\nu_2 + (v_3 + 1/2)h\nu_3 + x_{11}(v_1 + 1/2)^2 + x_{22}(v_2 + 1)^2 + x_{33}(v_3 + 1/2)^2 + x_{12}(v_1 + 1/2)(v_2 + 1) + x_{13}(v_1 + 1/2)(v_3 + 1/2) + x_{23}(v_2 + 1)(v_3 + 1/2) + hg_{22}l^2 + \cdots, \quad (5)$$

where v_i is the vibrational quantum number of mode i, x_{ij} the (cross) anharmonicity, l the vibrational angular momentum for the twofold degenerate ν_2 mode, and g_{22} the anharmonicity of the l states. The first line in the right-hand side of Eq. (5) contains the harmonic contributions, the second line the anharmonic ones, and the third line cross anharmonic and vibrational angular momentum contributions.

From the position of the peak in the CARS spectra one can determine the value of the cross anharmonicities. From Eq. (5) we see that ν_2 hot band peaks of the ν_1 mode are displaced by multiples of the cross anharmonicity x_{12}. The displacement between the (000)→(100) and the (010)→(110) peaks (as in Fig. 5) yield $x_{12} = -6.0\,cm^{-1}$. A comparison of this result with published cross anharmonicities[20–22] is shown in Table II.

Comparison of Figs. 5 and 6, taken at delay times of 200 ns and 4 μs, respectively, shows that at longer time delays extra small peaks appear between the ν_2 hot band peaks. These peaks are due to the collisional transfer of population to the excited states of the ν_3 mode, and can be attributed to the ν_3 hot band, i.e., (0,0,1)→(1,0,1),(0,1^1,1)→(1,1^1,1), etc. In analogy to the ν_2 hot band, these ν_3 hot band peaks are displaced from the ν_2 hot band peaks by the anharmonicity x_{13}. From the position of the small peaks it follows that $x_{13} = -2.7\,cm^{-1}$, which agrees well with literature values (see Table II).

TABLE II. Comparison of the cross anharmonicities of OCS obtained in this paper with published calculated and measured values. Data in Ref. 21 is from spontaneous Raman spectrum of liquid OCS.

	This work (cm^{-1})	Calculated Ref. 20	Measured Ref. 21	Measured Ref. 22
x_{12}	−6.0	−7.16	−7.0	−3.14
x_{13}	−2.7	−2.97	···	−2.53

Figure 9 shows that the temperature of the ν_2 mode continues to rise for 1 μs. This rise, which is relatively slow compared to the 250 ns FWHM duration of the CO_2 laser pulse, can be attributed to the long 1 μs tail of the laser pulse. In addition, Fig. 9 shows that a higher temperature is obtained at higher sample pressures. For short time delays the temperature increase is nearly linear with pressure, which implies that the excitation is enhanced by collisional processes. This collision assisted excitation can be understood as follows. First, pressure broadening helps compensate for the anharmonicity. Second, because the CO_2 laser is resonant with a specific rovibrational transition, the excitation creates a hole in the rotational manifold. Collisions redistribute the population in the rotational manifold, refilling the hole, thereby assisting the excitation and reducing saturation of the pumped transition. In addition to the collision assisted excitation, a faster decay in temperature is observed at high pressure, consistent with a collisional relaxation of the excitation energy to other modes and other degrees of freedom.

From the time dependence of the spectra one can obtain information on the vibrational relaxation rates. The fast relaxation of energy within the ν_2 mode is most clearly reflected by the fact that even though the laser populates the $v_2 = 2$ state, the population of the $v_2 = 1$ state always exceeds the population of the $v_2 = 2$ state. In general, the large population in the odd states implies that the energy transfer rate to those states exceeds the excitation rate. The observed equilibrium of energy of a time scale of 100 ns at 10 Torr provides a lower limit of $k_{\nu_2 \to \nu_2} \geqslant 1\ \mu s^{-1}\ Torr^{-1}$ for the collisional relaxation rate of the ν_2 mode. As a result of this fast relaxation most spectral reflect a Boltzmann distribution with a well-defined temperature, see for instance the closed circles in Fig. 8. At high excitation, however, the $v_2 = 0$ state was observed to have a lower population than predicted from a Boltzmann distribution (see, for instance, open circles in Fig. 8).

Energy transfer rates between ν_2 and the other vibrational modes have been reported in the literature.[13] The reported rate constants are $k_{\nu_2 \to \nu_3} = 12\ ms^{-1}\ Torr^{-1}$, and $k_{\nu_2 \to \nu_1} = 3.3\ ms^{-1}\ Torr^{-1}$. The appearance of the ν_3 peaks and the signal depletion discussed below are consistent with these relaxation rates. Finally, comparing Figs. 5 and 6, one notices that the peaks in Fig. 6 are more asymmetric. This can be attributed to population of higher rotational states at longer delay times because of relaxation of vibrational energy to the rotational degrees of freedom.

In addition to the large decrease of the ground state peak intensity upon infrared irradiation, there is an overall depletion of the CARS signal. This depletion can be seen by analyzing the area of the peaks in the CARS spectra in more detail. According to Eqs. (1) and (2) the square root of the area under each peak is proportional to the population difference between the $(0,v_2,0)$ and $(1,v_2,0)$ states. Figure 10 shows the ΔN obtained by taking the sum of the square root of the areas under each peak. Clearly, there is a decrease in the population difference of the first two states of the ν_1 mode as either the delay time or the pressure increases. This overall signal depletion, which is not unique to OCS, and which has been observed previously also for other molecules,[23,24] can be caused by a number of processes: dissociation, thermal lensing,[25,26] transfer of population to other modes, or to levels above $v_2 = 4$.

If dissociation occurs, it will result in signal depletion because of a reduced number of molecules in the probe region. Because of contradictory reports in the literature,[27,28] the possible occurrence of dissociation was investigated. Since maximum depletion is observed at high pressure, a 100 Torr sample was irradiated with 1.5×10^5 CO_2-laser pulses [irradiation volume: 10^{-3} cm^3; cell volume: 10 cm^3; fluence: 9.2 J/cm^2; laser line: $9P(24)$]. Subsequent Fourier transform infrared (FTIR) analysis, with a sensitivity of 100 ppm, showed no trace of CO, one of the dissociation products. This rules out dissociation as one of the possible causes for the observed signal depletion. Thermal lensing can also be ruled out, since the response time for this effect is the same as that for V–T relaxation (0.4 ms Torr)[25,26] which is significantly longer than the observed signal depletion rate.

The population of the levels above $v_2 = 4$ is not included in the calculation of ΔN in Fig. 10, because it cannot be determined directly from the CARS spectra. The population distributions in Fig. 8 nevertheless provide a method to estimate the fraction of molecules above this level; for a Boltzmann distribution at a temperature of 1500 K, this fraction is about 15%—much less than the 40% depletion of ΔN shown in Fig. 10. The appearance of the ν_3 hot band peaks in Fig. 6, however, shows that the $(v_1,v_2,v_3 = 1)$ states are populated. Since the CARS signal from the ν_2 hot band is proportional to $(N_{0,v_2,0} - N_{1,v_2,0})^2$ any energy transfer to states

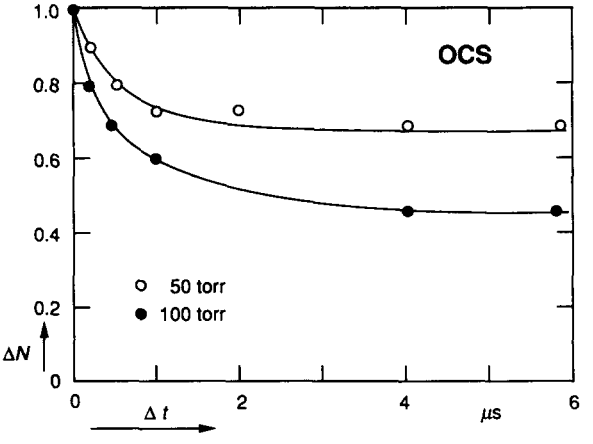

FIG. 10. The total population difference ΔN between the $(0,v_2,0)$ and $(1,v_2,0)$ states for $v_2 = (0,...,4)$ versus delay time after 9.2 J/cm^2 CO_2 laser excitation for different OCS pressures (O: 50 Torr, ●: 100 Torr).

other than $(0,v_2,0)$ will diminish the CARS signal. Therefore, the additional signal depletion in Fig. 10 must be attributed to transfer of energy to the ν_1 and ν_3 modes.

Finally, all spectra show that the $v_2 = 4$ peak is split into two peaks with a separation of 1.2 cm^{-1}. This splitting can be caused either by a Fermi resonance between $v_3 = 1$ and the $l = 0$ state of $v_2 = 4$ state,[29] or by the vibrational angular momentum splitting of the ν_2 mode. To distinguish between these two possibilities higher resolution data are required, for instance, using scanning instead of multiplex CARS. This would offer a very accurate method for determining either the state mixing in the case of a Fermi resonance, or the third order anharmonicity which results in a splitting of the l states.

VI. CONCLUSIONS

This paper presents a detailed study of the intramolecular vibrational energy distributions in infrared multiphoton excited OCS in the collisional regime using time-resolved multiplex coherent anti-Stokes spectroscopy. The anharmonicities x_{12} and x_{13}, the vibrational relaxation of the excitation energy to other degrees of freedom reported in this paper are consistent with values reported in the literature. The evolution of the spectra shows that the excitation energy rapidly equilibrates within the ν_2 pumped mode ($k_{\nu_2 \to \nu_2} \geqslant 1$ μs^{-1} $Torr^{-1}$), and that at all but the highest excitation the population in the ν_2 mode is well described by a Boltzmann distribution.

Coherent anti-Stokes Raman spectroscopy clearly is a powerful tool for the study of infrared multiphoton excitation. In addition to measuring other molecular systems and to studying pure rotational CARS spectra, several improvements of the current apparatus are currently in progress. First, measurements will be carried out in a molecular beam to ensure collisionless conditions. Second, shorter infrared excitation pulses will be employed, and, third subnanosecond time-resolution may be obtained on a single-shot basis by employing the time dispersion of the streak camera.

ACKNOWLEDGMENTS

We would like to thank Ms. Jian Wei for help with the dissociation measurements. This work was supported by the Army Research Office, under Contracts No. DAAL03-88-K-0114 and No. DAAL03-86-G-70098, and the Joint Services Electronics Program under Contract No. N00014-84-K-0465, and by Hamamatsu Photonics K.K.

[1] N. R. Isenor, V. Merchant, R. S. Hallsworth, and M. C. Richardson, Can. J. Phys. **51**, 1281 (1973).
[2] P. Esherick, A. J. Grimley, and A. Owyoung, Chem. Phys. **73**, 271 (1982).
[3] See, for example, Jyhpyng Wang, Kuei-Hsien Chen, and Eric Mazur, Phys. Rev. A **34**, 3892 (1986), and references therein.
[4] See, for example, D. W. Lupo and M. Quack, Chem. Rev. **87**, 181 (1987), and references therein.
[5] V. N. Bagratashvili, Yu. G. Vainer, V. S. Dolzhikov, S. F. Kol'yakov, V. S. Letokhov, A. A. Makarov, L. P. Malyavkin, E. A. Ryabov, E. G. Sil'kis, and V. D. Titov, Sov. Phys. JETP **53**, 512 (1981).
[6] See, for example, V. N. Bagratashvili, V. S. Letokhov, A. A. Makarov, and E. A. Ryabov, *Multiple Photon Infrared Laser Photophysics and Photochemistry* (Academic, New York, 1985).
[7] N. Bloembergen, *Nonlinear Optics* (Benjamin, New York, 1965); M. D. Levenson and Satoru S. Kano, *Introduction to Nonlinear Laser Spectroscopy*, revised edition (Academic, New York, 1988); Y. R. Shen, *The Principles of Nonlinear Optics* (Wiley, New York, 1984).
[8] R. V. Ambartsumyan, S. A. Akhmanov, A. M. Brodnikovskii, S. M. Gladkov, A. V. Evseev, V. N. Zadkov, M. G. Karimov, N. I. Koroteev, and A. A. Puretskii, JETP Lett. **35**, 210 (1982).
[9] S. S. Alimpiev, S. I. Valyanskii, S. M. Nikiforov, V. V. Smirnov, B. G. Sartakov, V. I. Fabelindkii, and A. L. Shtarkov, JETP Lett. **35**, 361 (1982).
[10] S. S. Alimpiev, A. A. Mokhnatyuk, S. M. Nikiforov, A. M. Prokhorov, B. G. Sartakov, V. V. Smirnov, and V. I. Fabelinskii, *Laser Spectroscopy VIII*, edited by W. Persson and S. Svanberg (Springer, Berlin, 1987), p. 229.
[11] J. A. Shirley, R. J. Hall, and A. C. Eckbreth, Opt. Lett. **5**, 380 (1980).
[12] W. B. Roh, P. W. Schreiber, and J. P. Taran, Appl. Phys. Lett. **29**, 174 (1976).
[13] M. L. Mandich and G. W. Flynn, J. Chem. Phys. **73**, 1265 (1980).
[14] J. W. Nibler and G. V. Kinghten, in *Raman Spectroscopy of Gases and Liquid*, edited by A. Weber (Springer, Berlin, 1979), p. 253.
[15] J. P. Taran, in *Raman Spectroscopy and Its Chemical Applications*, edited by W. Kiefer and D. A. Long (Reidel, Dordrecht, 1982), p. 281.
[16] M. D. Levenson and J. J. Song, in *Topics in Current Physics: Coherent Nonlinear Optics*, edited by M. S. Feld and V. S. Letokhov (Springer, Berlin, 1980), p. 293.
[17] A. C. Eckbreth and P. W. Schreiber, in *Chemical Application of Nonlinear Raman Spectroscopy*, edited by A. B. Harvey (Academic, New York, 1981), p. 27.
[18] Alan C. Eckbreth, Gregory M. Dobbs, John H. Stufflebeam, and Peter A. Tellex, Appl. Opt. **23**, 1328 (1984).
[19] F. Meyer-Bourbonneux, J. Dupre-Maquaire, and C. Meyer, J. Mol. Spectrosc. **63**, 288 (1976).
[20] A. Foord, J. G. Smith, and D. H. Whiffen, Mol. Phys. **29**, 1685 (1975).
[21] B. Hegemann and J. Jonas, J. Chem. Phys. **79**, 4683 (1983).
[22] Y. Morino and T. Nakagawa, J. Mol. Spectrosc. **26**, 496 (1968).
[23] E. L. Schweitzer and J. I. Steinfeld, Chem. Phys. **108**, 343 (1986).
[24] M. J. Shultz, L. M. Yam, and S. L. Berets, Spectrochimica Acta A **45**, 1 (1989).
[25] D. R. Siebert, F. R. Gradiner, and G. W. Flynn, J. Chem. Phys. **60**, 1564 (1974).
[26] K. M. Beck, A. Ringwelski, R. J. Gordon, Chem. Phys. Lett. **121**, 529 (1985).
[27] D. Proch and H. Schröder, Chem. Phys. Lett. **61**, 426 (1979).
[28] T. B. Simpson and N. Bloembergen, Optics Comm. **37**, 256 (1981).
[29] E. A. Triaille, J. Mol. Spectroc. **18**, 118 (1965).